Comparison of Different Compensation Methods of the Mutual Inductance for Self-Sensing Control

Niklas Himker, Georg Lindemann and Axel Mertens
Institute for Drive Systems and Power Electronics
Leibniz University Hannover
Hannover, Germany
niklas.himker@ial.uni-hannover.de, georg.lindemann@ial.uni-hannover.de, mertens@ial.uni-hannover.de

***Abstract*—A mutual inductance between the d-axis and q-axis leads to a stationary rotor position estimation error in a self-sensing control (SSC). In this paper, two methods to compensate the rotor position estimation error are compared. It is found that by considering the mutual inductance in an estimator for SSC based on numerical optimisation, the mutual inductance can be used as an source of information. Thus, the critical point, where the difference between the d-axis and q-axis inductances vanishes, can be operated with high position estimation quality in the presence of a mutual inductance. This is not possible with other methods for compensating the rotor position estimation error which are widely used in the literature.**

***Index Terms*—Cross-Coupling, Mutual Inductance, Permanent Magnet Synchronous Machine, Self-Sensing Control.**

I. Introduction

The inductance ratio makes the permanent magnet synchronous machine (PMSM) suitable for anisotropy-based self-sensing control (SSC) at low speeds. Anisotropy-based SSC evaluate the response of the PMSM to an injected signal, allowing the rotor position to be estimated using various methods (e.g., [1], [2]).

It is well known that a mutual inductance, which leads to a cross-coupling, results in an error of the estimated rotor position [3]. A non-zero mutual inductance introduces a reaction to an injected d-axis voltage also in the q-axis. In effect, the estimated rotor position is rotated until the expected property of a correct orientation arises (the impressed current is in the same direction as the injected voltage). This results in a rotor position estimation error of

$$\gamma_{\mathrm{err}} = -\frac{1}{2}\mathrm{atan}\left(\frac{L'_{\mathrm{dq}}}{\Delta L'}\right) \tag{1}$$

if an alternating signal is used. This corresponds to a twist of the anisotropy [4], [5].

This error can be compensated if the mutual inductance and self-inductances of the PMSM are known, as explained in [6]. For this, the initial value of the rotor position estimation is corrected by the expected rotor position estimation error before being used in the motor control. In a simple case, this can be done as a function of the q-current [7].

Alternatively, an estimator was presented in [8] which, with known mutual inductance and self-inductances of the PMSM, already takes into account the mutual inductance in the expected response, leading to a correct estimate of the rotor position. This is achieved by numerical optimisation based on the voltage differential equation of the PMSM, since the inductance matrix including the mutual inductance is used in the calculation of the residual for the numerical optimisation. The flux derivative estimator (FDE) with quasi-direct (QD) calculation according to [8] is used as the rotor position estimator in this work.

These two methods, the rotation by the expected rotor position estimation error and the inclusion of the mutual inductance in the numerical optimisation, are compared in this paper. In contrast to the quality criterion for the suitability of PMSM for anisotropy-based SSC established in [4], it is shown that the mutual inductance can be used as additional information even if the self-inductances of the d-axis and q-axis are identical. This widens the field of suitable PMSMs for SSC. In addition, a mutual inductance can be intentionally introduced into the machine design to improve the suitability of PMSMs, instead of reducing the mutual inductance (as explained in [9]), in order to ride through the point with identical self-inductances of the d-axis and q-axis.

At the beginning of the paper, the fundamentals are presented, whereby both the machine model and the numerical optimisation method are introduced. Then, the behaviour of the SSC in the presence of mutual inductance is compared in simulation, first without and then with the two compensation methods. Experimental results validate the functionality of the SSC in the presence of mutual inductance.

II. Fundamentals

In the following, the model of the PMSM and the adaptation law of the SSC with numerical optimisation are presented.

A. Model of the PMSM

The model of the PMSM in the dq-reference frame is derived in [8], leading to

$${}^{(\mathrm{dq})}\vec{v} = R\,{}^{(\mathrm{dq})}\vec{i} + \mathbf{L}'_{(\mathrm{dq})}\frac{\mathrm{d}}{\mathrm{d}t}{}^{(\mathrm{dq})}\vec{i}_{\Sigma} + \mathbf{J}\omega_{\mathrm{el}}\mathbf{L}_{(\mathrm{dq})}\,{}^{(\mathrm{dq})}\vec{i} + {}^{(\mathrm{dq})}\vec{v}_{\mathrm{EMF}} \tag{2}$$

with

$$\omega_{\mathrm{el}} = \frac{\mathrm{d}}{\mathrm{d}t}\gamma_{\mathrm{el}}\ ,\ \mathbf{J} = \begin{pmatrix} 0 & -1 \\ 1 & 0 \end{pmatrix}\ \text{and}\ {}^{(\mathrm{dq})}\vec{v}_{\mathrm{EMF}} = \omega_{\mathrm{el}}\Psi_{\mathrm{PM}}\begin{pmatrix} 0 \\ 1 \end{pmatrix}\ . \tag{3}$$

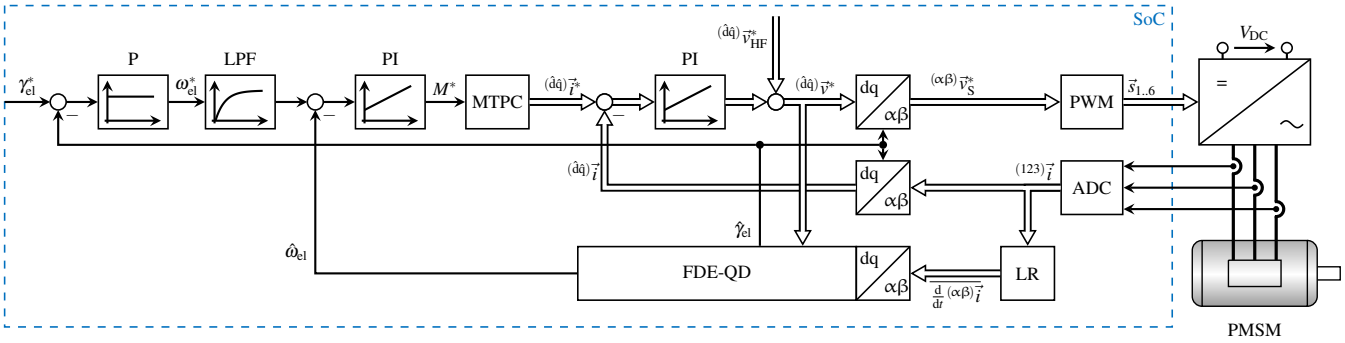

Figure 1: Block diagram of the SSC used with PMSM and converter (encoder for benchmarking is not shown)

The voltage in the dq-reference frame is ${}^{(\mathrm{dq})}\vec{v}$ and the current is ${}^{(\mathrm{dq})}\vec{i}$. The flux of the permanent magnet is Ψ_{PM} and R is the stator resistance of the machine. The rotor position is γ_{el}, and the angular speed of the machine is ω_{el}. The current-dependent secant inductance is

$$\mathbf{L}_{(\mathrm{dq})}\left({}^{(\mathrm{dq})}\vec{i}\right) = \begin{pmatrix} L_{\mathrm{d}}\left({}^{(\mathrm{dq})}\vec{i}\right) & L_{\mathrm{dq}}\left({}^{(\mathrm{dq})}\vec{i}\right) \\ L_{\mathrm{dq}}\left({}^{(\mathrm{dq})}\vec{i}\right) & L_{\mathrm{q}}\left({}^{(\mathrm{dq})}\vec{i}\right) \end{pmatrix} \tag{4}$$

with the self-inductances L_{d} and L_{q} and the mutual inductance L_{dq}. The current dependent differential inductance

$$\mathbf{L}'_{(\mathrm{dq})}\left({}^{(\mathrm{dq})}\vec{i}\right) := \frac{\mathrm{d}^{(\mathrm{dq})}\vec{\Psi}}{\mathrm{d}^{(\mathrm{dq})}\vec{i}} \tag{5}$$

$$\begin{pmatrix} L'_{\mathrm{d}}\left({}^{(\mathrm{dq})}\vec{i}\right) & L'_{\mathrm{dq}}\left({}^{(\mathrm{dq})}\vec{i}\right) \\ L'_{\mathrm{dq}}\left({}^{(\mathrm{dq})}\vec{i}\right) & L'_{\mathrm{q}}\left({}^{(\mathrm{dq})}\vec{i}\right) \end{pmatrix} := \begin{pmatrix} \frac{\partial \Psi_{\mathrm{d}}}{\partial i_{\mathrm{d}}} & \frac{\partial \Psi_{\mathrm{d}}}{\partial i_{\mathrm{q}}} \\ \frac{\partial \Psi_{\mathrm{q}}}{\partial i_{\mathrm{d}}} & \frac{\partial \Psi_{\mathrm{q}}}{\partial i_{\mathrm{q}}} \end{pmatrix}$$

is used. The differential self-inductances of the d-axis and q-axis are L'_{d} and L'_{q}, respectively, and the mutual inductance is L'_{dq}. For the current dependent inductance matrices, we introduce the abbreviation

$$\mathbf{L}_{(\mathrm{dq})} := \mathbf{L}_{(\mathrm{dq})}\left({}^{(\mathrm{dq})}\vec{i}\right) \quad \text{and} \quad \mathbf{L}'_{(\mathrm{dq})} := \mathbf{L}'_{(\mathrm{dq})}\left({}^{(\mathrm{dq})}\vec{i}\right) \quad . \tag{6}$$

Additionally, the rotor position error

$$\gamma_{\mathrm{err}} = \gamma_{\mathrm{el}} - \hat{\gamma}_{\mathrm{el}} \tag{7}$$

with the estimated rotor position $\hat{\gamma}_{\mathrm{el}}$ is defined.

B. Quasi-Direct Position Estimation

The QD algorithm of [8], [10] with the nomenclature of [10] is used. The adaption law of the QD algorithm is defined with

$$\begin{aligned} \hat{\gamma}_{\mathrm{err}}(k,i+1) = \hat{\gamma}_{\mathrm{err}}(k,i) \\ -\frac{\eta}{2^{i-1}}\,\mathrm{sgn}\Big[\left(J_{\mathrm{FDE}}\left(\hat{\gamma}_{\mathrm{err}}(k,i)\right)^T J_{\mathrm{FDE}}\left(\hat{\gamma}_{\mathrm{err}}(k,i)\right)\right)^{-1} \\ \cdot J_{\mathrm{FDE}}\left(\hat{\gamma}_{\mathrm{err}}(k,i)\right)^T\, {}^{(\hat{\mathrm{dq}})}\vec{r}_{\mathrm{FDE}}\left(\hat{\gamma}_{\mathrm{err}}(k,i)\right)\Big] \quad . \end{aligned} \tag{8}$$

The operator for a discrete sample is k. The Jacobian matrix is given by

$$J_{\mathrm{FDE}}\left(\hat{\gamma}_{\mathrm{err}}\right) = \begin{pmatrix} \frac{\partial r_{\mathrm{d,FIE}}}{\partial \hat{\gamma}_{\mathrm{err}}} \\ \frac{\partial r_{\mathrm{q,FIE}}}{\partial \hat{\gamma}_{\mathrm{err}}} \end{pmatrix} = \frac{\partial}{\partial \hat{\gamma}_{\mathrm{err}}}\,{}^{(\hat{\mathrm{dq}})}\vec{r}_{\mathrm{FDE}} \quad . \tag{9}$$

The residual ${}^{(\hat{\mathrm{dq}})}\vec{r}_{\mathrm{FDE}}$ is derived in the next chapter. A basic structure of the QD calculation is shown in Fig. 2. Equation (8) is solved iteratively with the counter i and the calling rate of the QD calculation is f_{QD}. The speed is estimated via an integrator with the time constant $T_{\mathrm{QD,I}}$ [8]. The estimated speed is also used to feed-forward the position change of each call of the estimator via the angle γ_{step}.

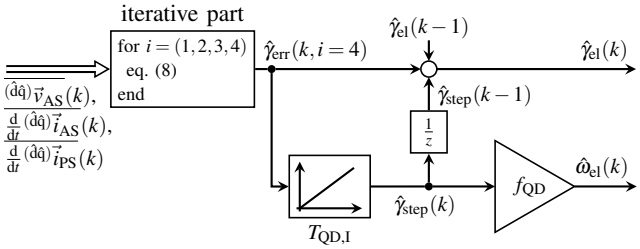

Figure 2: Structure of the QD calculation [10]

The block diagram of the field-oriented control using the SSC based on an estimator using the QD calculation is shown in Fig. 1.

III. Comparison of the Residual with and without a Mutual Inductance

After the adaptation law of the numerical optimisation has been presented, the residual is introduced with and without consideration of the mutual inductance.

A. Residual with Consideration of a Mutual Inductance

The residual of the FDE is derived from the flux derivative of the PMSM during a pulse-width modulation (PWM) period. Example voltage and current waveforms of the d-axis are shown in Fig. 3. In the upper row, the voltage provided by the inverter can be seen. The resulting current response is displayed below. The average voltage $v_{\mathrm{d,AS}}$ during an active switching state (AS), the current slope in the AS $\overline{\frac{\mathrm{d}}{\mathrm{d}t} i_{\mathrm{d,AS}}}$ and also the current slope in the passive switching state (PS) $\overline{\frac{\mathrm{d}}{\mathrm{d}t} i_{\mathrm{q,PS}}}$

are highlighted in different colours. For the PS, the differential equation of the PMSM results in

$$0 = \underbrace{R\overline{{}^{(\hat{d}\hat{q})}\vec{i}_{PS}} + \omega_{el}\mathbf{J}\mathbf{L}_{(dq)}\overline{{}^{(\hat{d}\hat{q})}\vec{i}_{PS}} + \overline{{}^{(\hat{d}\hat{q})}\vec{v}_{EMF,PS}}}_{\overline{{}^{(\hat{d}\hat{q})}\vec{v}_{fm,PS}}} + \mathbf{L}'_{(dq)}\overline{\frac{d}{dt}{}^{(\hat{d}\hat{q})}\vec{i}_{PS}} \quad . \tag{10}$$

The differential equation of the AS results in

$$0 = \underbrace{R\overline{{}^{(\hat{d}\hat{q})}\vec{i}_{AS}} + \omega_{el}\mathbf{J}\mathbf{L}_{(dq)}\overline{{}^{(\hat{d}\hat{q})}\vec{i}_{AS}} + \overline{{}^{(\hat{d}\hat{q})}\vec{v}_{EMF,AS}}}_{\overline{{}^{(\hat{d}\hat{q})}\vec{v}_{fm,AS}}} + \mathbf{L}'_{(dq)}\overline{\frac{d}{dt}{}^{(\hat{d}\hat{q})}\vec{i}_{AS}} - \overline{{}^{(\hat{d}\hat{q})}\vec{v}_{AS}} \quad . \tag{11}$$

In the programmable logic (PL), the current derivative of the PS $\overline{{}^{(\hat{d}\hat{q})}\vec{i}_{PS}}$ is measured with a linear regression (LR) algorithm. The voltages $\overline{{}^{(\hat{d}\hat{q})}\vec{v}_{fm,PS}}$ and $\overline{{}^{(\hat{d}\hat{q})}\vec{v}_{fm,AS}}$ are the fundamental components of the differential equation. The current derivative of the AS can be calculated using the results of two consecutive PS.

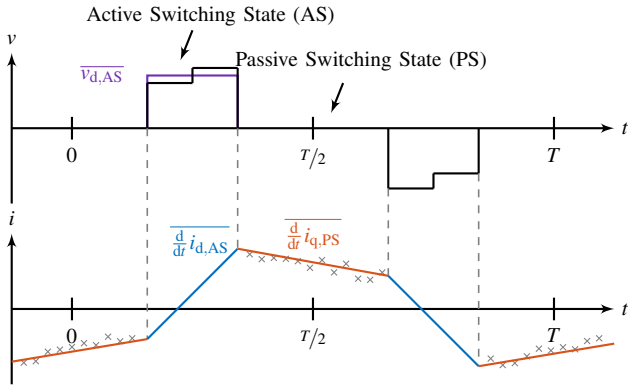

Figure 3: Voltage and current during a PWM period with square-wave injection [8]

The FDE uses a consecutive PS and AS [8]. The assumption

$$\mathbf{L}'_{(\hat{d}\hat{q})}\overline{\frac{d}{dt}{}^{(\hat{d}\hat{q})}\vec{i}_{PS}} = -\overline{{}^{(\hat{d}\hat{q})}\vec{v}_{fm,PS}} = -\overline{{}^{(\hat{d}\hat{q})}\vec{v}_{fm,AS}} \tag{12}$$

is made. Substituting the voltage $\overline{{}^{(\hat{d}\hat{q})}\vec{v}_{fm,AS}}$ into (11) with $-\mathbf{L}'_{(\hat{d}\hat{q})}\overline{\frac{d}{dt}{}^{(\hat{d}\hat{q})}\vec{i}_{PS}}$ yields the residual of the FDE

$${}^{(\hat{d}\hat{q})}\vec{r}_{FDE} = \overline{{}^{(\hat{d}\hat{q})}\vec{v}_{AS}} + \mathbf{L}'_{(\hat{d}\hat{q})}\overline{\frac{d}{dt}{}^{(\hat{d}\hat{q})}\vec{i}_{PS}} - \mathbf{L}'_{(\hat{d}\hat{q})}\overline{\frac{d}{dt}{}^{(\hat{d}\hat{q})}\vec{i}_{AS}} \quad . \tag{13}$$

In the next step, the Jacobian matrix is derived analytically. For this, the inductance matrix in the $\hat{d}\hat{q}$-reference frame

$$\mathbf{L}_{(\hat{d}\hat{q})} = \Sigma L' \begin{pmatrix} 1 & 0 \\ 0 & 1 \end{pmatrix} + \Delta L' \begin{pmatrix} \cos(2\gamma_{err}) & \sin(2\gamma_{err}) \\ \sin(2\gamma_{err}) & -\cos(2\gamma_{err}) \end{pmatrix} + L'_{dq} \begin{pmatrix} -\sin(2\gamma_{err}) & \cos(2\gamma_{err}) \\ \cos(2\gamma_{err}) & \sin(2\gamma_{err}) \end{pmatrix} \tag{14}$$

with

$$\Sigma L' = \frac{L'_d + L'_q}{2} \quad \text{and} \quad \Delta L' = \frac{L'_d - L'_q}{2} \tag{15}$$

is used. This inductance matrix is simplified by an approximation which assumes small estimation errors

$$\mathbf{L}_{(\hat{d}\hat{q})} = \begin{pmatrix} L'_d & L'_{dq} \\ L'_{dq} & L'_q \end{pmatrix} + 2\gamma_{err} \begin{pmatrix} -L'_{dq} & \Delta L' \\ \Delta L' & L'_{dq} \end{pmatrix} \quad . \tag{16}$$

The Jacobian matrix results in

$$J_{FDE}(\hat{\gamma}_{err}) = \begin{pmatrix} \frac{\partial r_{d,FDE}}{\partial \hat{\gamma}_{err}} \\ \frac{\partial r_{q,FDE}}{\partial \hat{\gamma}_{err}} \end{pmatrix} = \frac{\partial}{\partial \hat{\gamma}_{err}}{}^{(\hat{d}\hat{q})}\vec{r}_{FDE} = 2\begin{pmatrix} -L'_{dq} & \Delta L' \\ \Delta L' & L'_{dq} \end{pmatrix} \left(\overline{\frac{d}{dt}{}^{(\hat{d}\hat{q})}\vec{i}_{PS}} - \overline{\frac{d}{dt}{}^{(\hat{d}\hat{q})}\vec{i}_{AS}} \right) \quad . \tag{17}$$

The adaption law of the parameter optimisation according to [10] leads to

$$\hat{\gamma}_{err}(i+1) = \hat{\gamma}_{err}(i) - \frac{\eta}{2^{i-1}}\,\mathrm{sgn}\left[J_{FDE}(\hat{\gamma}_{err})^T\, {}^{(\hat{d}\hat{q})}\vec{r}_{FDE} \right] \quad . \tag{18}$$

In (18), the denominator of (8)

$$\left(J_{FDE}(\hat{\gamma}_{err}(k,i))^T J_{FDE}(\hat{\gamma}_{err}(k,i)) \right)^{-1} = \frac{1}{\left(\frac{\partial r_{d,FDE}}{\partial \hat{\gamma}_{err}}\right)^2 + \left(\frac{\partial r_{q,FDE}}{\partial \hat{\gamma}_{err}}\right)^2} \tag{19}$$

within the signum function is neglected, due to it always being positive.

B. Residual without Consideration of a Mutual Inductance

For the comparison with an estimator without using the mutual inductances, the residual yields

$${}^{(\hat{d}\hat{q})}\tilde{\vec{r}}_{FDE} = \overline{{}^{(\hat{d}\hat{q})}\vec{v}_{AS}} + \tilde{\mathbf{L}}'_{(\hat{d}\hat{q})}\overline{\frac{d}{dt}{}^{(\hat{d}\hat{q})}\vec{i}_{PS}} - \tilde{\mathbf{L}}'_{(\hat{d}\hat{q})}\overline{\frac{d}{dt}{}^{(\hat{d}\hat{q})}\vec{i}_{AS}} \tag{20}$$

with

$$\tilde{\mathbf{L}}'_{(\hat{d}\hat{q})} = \Sigma L' \begin{pmatrix} 1 & 0 \\ 0 & 1 \end{pmatrix} + \Delta L' \begin{pmatrix} \cos(2\gamma_{err}) & \sin(2\gamma_{err}) \\ \sin(2\gamma_{err}) & -\cos(2\gamma_{err}) \end{pmatrix} \tag{21}$$

and its Jacobian is

$$\tilde{J}_{FDE}(\hat{\gamma}_{err}) = \begin{pmatrix} \frac{\partial \tilde{r}_{d,FDE}}{\partial \hat{\gamma}_{err}} \\ \frac{\partial \tilde{r}_{q,FDE}}{\partial \hat{\gamma}_{err}} \end{pmatrix} = \frac{\partial}{\partial \hat{\gamma}_{err}}{}^{(\hat{d}\hat{q})}\tilde{\vec{r}}_{FDE} = 2\begin{pmatrix} 0 & \Delta L' \\ \Delta L' & 0 \end{pmatrix} \left(\overline{\frac{d}{dt}{}^{(\hat{d}\hat{q})}\vec{i}_{PS}} - \overline{\frac{d}{dt}{}^{(\hat{d}\hat{q})}\vec{i}_{AS}} \right). \tag{22}$$

Analogous to the residual with the mutual inductance, the simplification for small estimation errors is used.

To calculate the expected error due to a mutual inductance, the current derivative

$$\overline{\frac{d}{dt}{}^{(\hat{d}\hat{q})}\vec{i}_{\Sigma}} = \overline{\frac{d}{dt}{}^{(\hat{d}\hat{q})}\vec{i}_{PS}} - \overline{\frac{d}{dt}{}^{(\hat{d}\hat{q})}\vec{i}_{AS}} \tag{23}$$

is used. This current derivative can be calculated using the inductance matrix in the estimated reference frame

$$\overline{\frac{d}{dt}{}^{(\hat{d}\hat{q})}\vec{i}_{\Sigma}} = -\frac{1}{L'_{\hat{d}}L'_{\hat{q}} - L'^{\,2}_{\hat{d}\hat{q}}} \begin{pmatrix} L'_{\hat{q}} & -L'_{\hat{d}\hat{q}} \\ -L'_{\hat{d}\hat{q}} & L'_{\hat{d}} \end{pmatrix} {}^{(\hat{d}\hat{q})}\vec{v}^{*}_{HF} \tag{24}$$

with

$$L'_{\hat{\mathrm{d}}} = \Sigma L' + \Delta L' \cos\left(2\gamma_{\mathrm{err}}\right) - L'_{\mathrm{dq}} \sin\left(2\gamma_{\mathrm{err}}\right) \tag{25}$$

$$L'_{\hat{\mathrm{q}}} = \Sigma L' - \Delta L' \cos\left(2\gamma_{\mathrm{err}}\right) + L'_{\mathrm{dq}} \sin\left(2\gamma_{\mathrm{err}}\right) \tag{26}$$

and

$$L'_{\hat{\mathrm{d}}\hat{\mathrm{q}}} = L'_{\mathrm{dq}} \cos\left(2\gamma_{\mathrm{err}}\right) + \Delta L' \sin\left(2\gamma_{\mathrm{err}}\right) \quad . \tag{27}$$

For the q-axis, the current derivative results in

$$\frac{\mathrm{d}}{\mathrm{d}t} i_{\hat{\mathrm{q}},\Sigma} = -\frac{L'_{\hat{\mathrm{d}}\hat{\mathrm{q}}} v_{\hat{\mathrm{d}},\mathrm{hf}}}{L'_{\hat{\mathrm{d}}} L'_{\hat{\mathrm{q}}} - L'^{\,2}_{\hat{\mathrm{d}}\hat{\mathrm{q}}}} \quad , \tag{28}$$

if only the d-axis is excited with a test signal. With no mutual inductance the current derivative of the q-axis is expected to be zero, yielding

$$0 \stackrel{!}{=} -\frac{L'_{\hat{\mathrm{d}}\hat{\mathrm{q}}} v_{\hat{\mathrm{d}},\mathrm{hf}}}{L'_{\hat{\mathrm{d}}} L'_{\hat{\mathrm{q}}} - L'^{\,2}_{\hat{\mathrm{d}}\hat{\mathrm{q}}}} \quad . \tag{29}$$

In Fig. 4, this search is visualised in three steps.

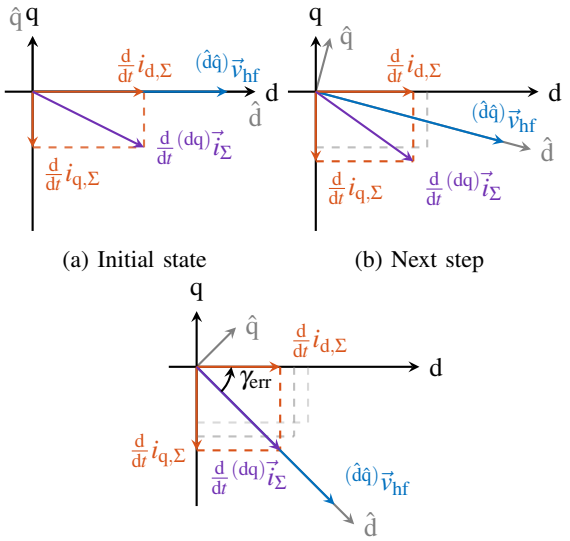

(a) Initial state (b) Next step

(c) Stationary state

Figure 4: Progression of the rotor position estimation in the presence of a positive mutual inductance, without using the mutual inductance in the residual ${}^{(\hat{\mathrm{dq}})}\vec{r}_{\mathrm{FDE}}$

From the initial state, the current derivative of the estimated q-axis is not equal to zero. The estimator then changes the estimated reference frame and the test signal is injected into a falsely estimated axis. This is repeated until the current derivative of the estimated q-axis is equal to zero, which is shown in the stationary state.

By analysing (29), the requirement for a stationary estimation

$$0 \stackrel{!}{=} L'_{\hat{\mathrm{d}}\hat{\mathrm{q}}} \quad , \tag{30}$$

is derived. Thus, the estimator searches for the point at which (27) becomes zero:

$$0 \stackrel{!}{=} L'_{\mathrm{dq}} \cos\left(2\gamma_{\mathrm{err}}\right) + \Delta L' \sin\left(2\gamma_{\mathrm{err}}\right) \quad . \tag{31}$$

This can be rearranged to give

$$\frac{\sin\left(2\gamma_{\mathrm{err}}\right)}{\cos\left(2\gamma_{\mathrm{err}}\right)} = -\frac{L'_{\mathrm{dq}}}{\Delta L'} \quad . \tag{32}$$

Using an estimator which does not account for a mutual inductance and uses an alternating signal for estimation, the stationary estimation error results in

$$\gamma_{\mathrm{err}} = -\frac{1}{2} \mathrm{atan}\left(\frac{L'_{\mathrm{dq}}}{\Delta L'}\right) \quad , \tag{33}$$

which is widely known in the literature [4], [11].

From the known error, the true rotor position is approximated by

$$\tilde{\gamma}_{\mathrm{el}} = \hat{\gamma}_{\mathrm{el}} + \frac{1}{2} \mathrm{atan}\left(\frac{L'_{\mathrm{dq}}}{\Delta L'}\right) = \hat{\gamma}_{\mathrm{el}} + \tilde{\gamma}_{\mathrm{MI}} \quad . \tag{34}$$

IV. Simulation Results

Within simulations, the effect of a mutual inductance on the rotor position estimation and the compensation methods is investigated. In Fig. 5, a test case is presented where the rotor of the PMSM is locked. The dynamic response of the rotor position estimation error is shown by a setpoint step change of the q-current. The change of the q-current leads to a change in the mutual inductance in the interval $L'_{\mathrm{dq}} = [0, \ldots, 9.5]\,\mu\mathrm{H}$.

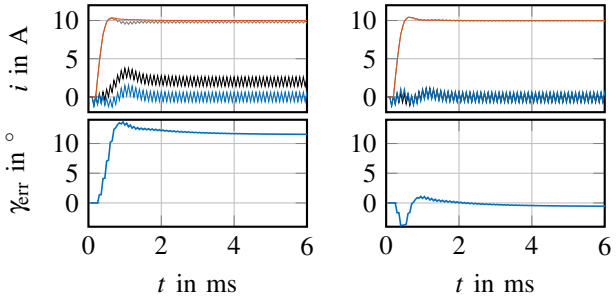

(a) Without compensation (b) Compensation via $\tilde{\gamma}_{\mathrm{MI}}$

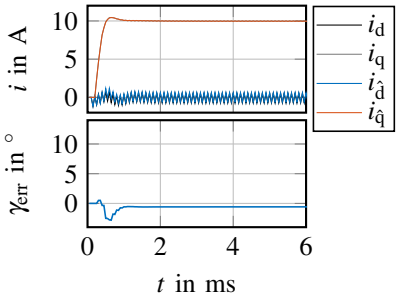

(c) Compensation via L'_{dq} in ${}^{(\hat{\mathrm{dq}})}\vec{r}_{\mathrm{FDE}}$

Figure 5: Comparison of the rotor position error for the different compensations methods with $L'_{\mathrm{d}}\left(i_{\mathrm{q}} = 10\,\mathrm{A}\right) = 205\,\mu\mathrm{H}$, $L'_{\mathrm{q}}\left(i_{\mathrm{q}} = 10\,\mathrm{A}\right) = 250\,\mu\mathrm{H}$ and $L'_{\mathrm{dq}}\left(i_{\mathrm{q}} = 10\,\mathrm{A}\right) = 9.5\,\mu\mathrm{H}$

In Fig. 5(a), the mutual inductance is not compensated, resulting in a stationary rotor position estimation error of 12°. When compensating the mutual inductance in Fig. 5(b)

and Fig. 5(c), no stationary rotor position estimation error remains. Differences only arise in the dynamic region. The rotor position estimation error with compensation for the pre-calculated error $\tilde{\gamma}_{\mathrm{MI}}$ shows a higher magnitude compared to the method from Fig. 5(c). Furthermore, the plots of the rotor position estimation error in Fig. 5(a) and Fig. 5(b) show a longer transient response than the method in Fig. 5(c).

Next, the steady-state behaviour of the rotor position estimate is investigated for different combinations of the difference of the self-inductances $\Delta L'$ and the mutual inductance L'_{dq}. In the simulation, an electrical rotor revolution is simulated and the root-mean-square value of the rotor position estimation error $\gamma_{\mathrm{er,RMS}}$ is plotted. In Fig. 6(a), the result with the feed-forward angle $\tilde{\gamma}_{\mathrm{MI}}$ is shown. Rotor position estimation errors with magnitudes greater than 5° are clipped. As expected from the state of the art, the rotor position estimation fails for the case where the difference in the self-inductances is $\Delta L' = 0$. For the variant which considers the mutual inductance in the residual, the result is shown in Fig. 6(b). A rotor position estimate at $\Delta L' = 0$ is possible as long as the magnitude of the mutual inductance L'_{dq} is sufficiently large. Only if the difference of the self-inductances $\Delta L'$ and the mutual inductance L'_{dq} are both close to zero, the rotor position estimation becomes unstable.

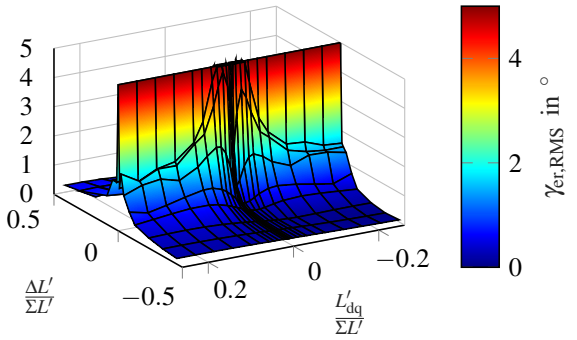

(a) Compensation via $\tilde{\gamma}_{\mathrm{MI}}$

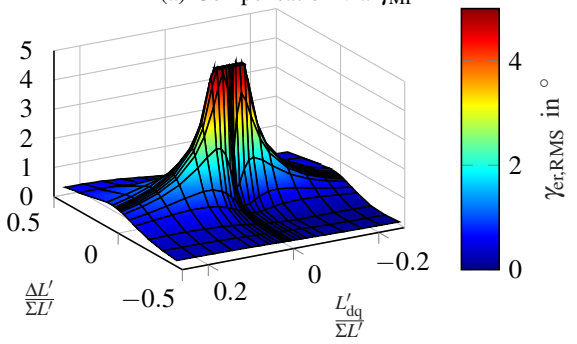

(b) Compensation via L'_{dq} in ${}^{(\hat{\mathrm{dq}})}\vec{r}_{\mathrm{FDE}}$

Figure 6: Comparison of the root-mean-square value of the rotor position error for the different compensations methods against different values of the difference of the self-inductances $\Delta L'$ and the mutual inductance L'_{dq}

Next, the ride through of identical self-inductances ($\Delta L' = 0$) is simulated and the variant with pre-rotation through $\tilde{\gamma}_{\mathrm{MI}}$ is compared with the variant which considers the mutual inductance in the residual. The results are shown in Fig. 7. The setup corresponds to that of Fig. 5, with the actual values of the inductances added. Moreover, the machine parameters are synthetic values, so that the staircase-like increase of the q-current to $i_{\mathrm{q}} = 10\,\mathrm{A}$ results in identical self-inductances ($\Delta L' = 0$) and sufficient mutual inductance at $i_{\mathrm{q}} = 5\,\mathrm{A}$.

As shown by the curve of the rotor position estimation error without compensation of the mutual inductance in Fig. 7(a), the rotor position estimation error increases to 45° until the point with identical self-inductances at $i_{\mathrm{q}} = 5\,\mathrm{A}$ is reached. As the q-current is increased further, the rotor position estimation error changes to -135° and the rotor position estimation becomes unstable. This happens at an estimated q-current of $i_{\hat{\mathrm{q}}} \approx 7\,\mathrm{A}$.

If the mutual inductance is compensated by rotation through $\tilde{\gamma}_{\mathrm{MI}}$, the rotor position estimation error remains small with increasing q-current until the point with identical self-inductances is reached at $i_{\mathrm{q}} = 5\,\mathrm{A}$. Here, the rotor position estimation becomes unstable until a q-current of $i_{\mathrm{q}} > 5\,\mathrm{A}$ is imposed and a difference in self-inductances is present. In the range with small differences of the self-inductances, the estimated rotor position is noisy.

Using L'_{dq} in the residual of the estimator, the rotor position estimate remains stable at every point and the rotor position estimation error remains smaller than 3°. As an overall result, the variant which considers the mutual inductance in the residual remains stable and the variants with rotation through $\tilde{\gamma}_{\mathrm{MI}}$ and without compensation become unstable.

V. Experimental Validation

For the experimental investigation, the estimator is implemented on the rapid prototyping system of [8]. The analogue-to-digital converters (ADCs) for shunt-based current measurement are driven by the PL with a sampling frequency of 1 MHz. The estimator is executed once per PWM period ($f_{\mathrm{EST}} = f_{\mathrm{PWM}} = 10\,\mathrm{kHz}$). The speed controller is executed with $f_{\mathrm{speed}} = 5\,\mathrm{kHz}$. The PWM generator controls the MOSFET-based inverter with a DC-link voltage of 48 V.

The parameters associated with the PMSM used are given in Table I, and the current dependent differential inductance is shown in Fig. 8.

TABLE I
PMSM rated values and machine data

Rated current (RMS)	I_{r}	6.7 A
Rated torque	M_{r}	0.5 Nm
Rated rotational speed	n_{r}	5850 min^{-1}
Phase resistance	R	0.39 Ω
Flux linkage	Ψ_{PM}	8.05 mVs
Number of pole pairs	p	4

As seen in Fig. 8, it is not possible to drive through identical self-inductances ($\Delta L' = 0$), because this saturation state cannot be reached with the device under test. Thus, only a proof of concept can be shown on the test bench. The parameters regarding the control and estimator are given in Table II.

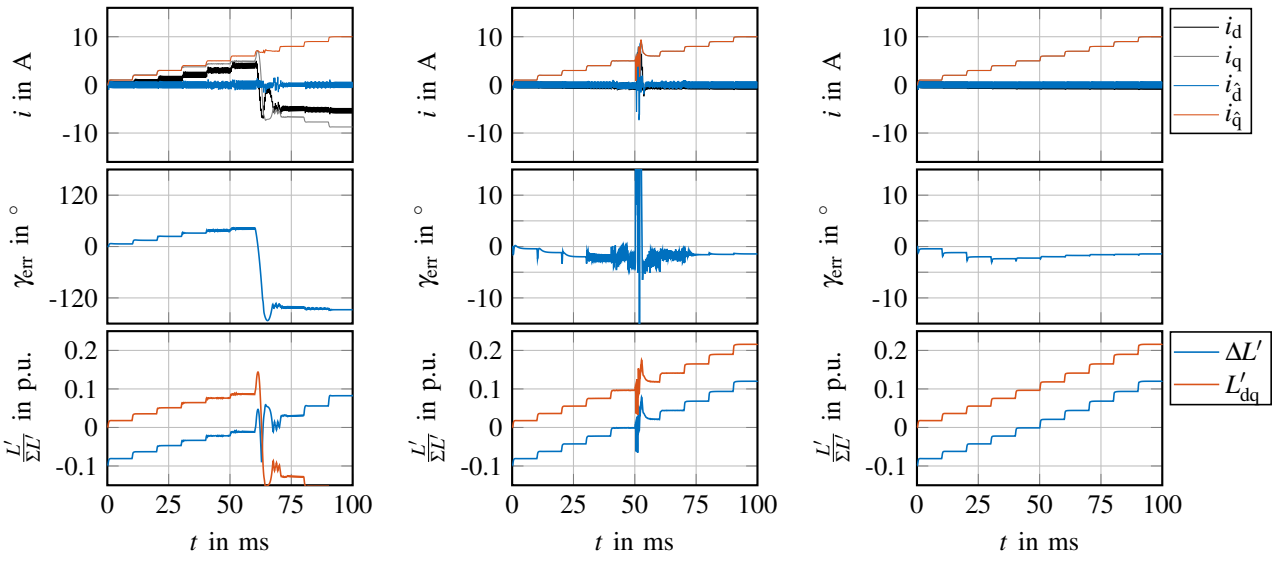

(a) Without compensation (b) Compensation via $\tilde{\gamma}_{\mathrm{MI}}$ (c) Compensation via L'_{dq} in ${}^{(\hat{\mathrm{dq}})}\vec{r}_{\mathrm{FDE}}$

Figure 7: Comparison of the different compensation methods while drive through identical self-inductances ($\Delta L' = 0$) with sufficient mutual inductance $L_{(\mathrm{dq})}$

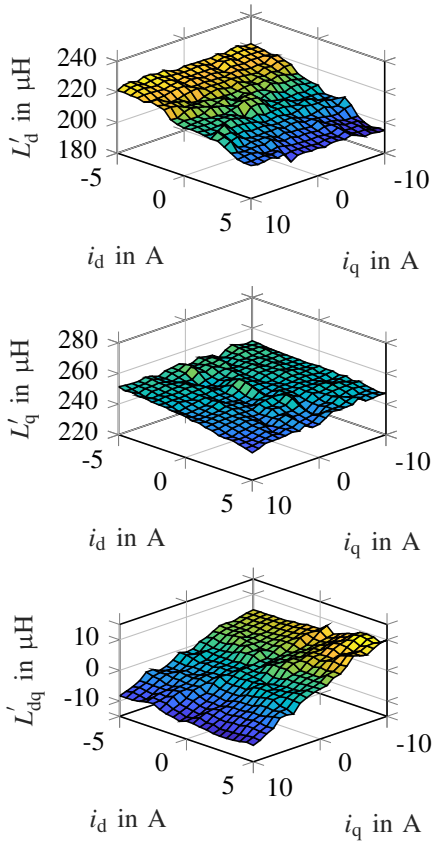

Figure 8: Measured differential inductances of the PMSM

As a test scenario, the device under test is position controlled to $\hat{\gamma}_{\mathrm{el}} = 0°$. The load machine applies the positive rated torque, reverses the torque and sets the torque back to zero.

TABLE II
Control and estimator parameters used

P-gain current control	$K_{\mathrm{i,P}}$	1.5 $\mathrm{V/A}$
Time const. current control	$T_{\mathrm{i,N}}$	0.5 ms
Iterations	l_{QD}	4
Initial step width	η	$5.4 \cdot 10^{-3}$ rad
Integrator time const.	$T_{\mathrm{QD,I}}$	3.3 ms
Square-wave injection amplitude	v_{hf}	5 V
P-gain speed control	$K_{\omega,\mathrm{P}}$	0.061 A · min
Time const. speed control	$T_{\omega,\mathrm{N}}$	15.9 ms
P-gain position control	$K_{\gamma,\mathrm{P}}$	70 $\frac{1}{\mathrm{rad \cdot min}}$

As a result, the rotor position changes with each load step and is brought back to the reference value by the position controller. The result without compensation is shown in Fig. 9. In the first row, the currents of the PMSM are shown. This is followed by the estimated and measured positions. Below this, the rotor position error is shown. In the last row, the estimated and measured speeds are displayed.

Looking at the estimated position, the controller maintains the estimated position in the steady states at 0°, but a rotor position error corresponding to the uncompensated mutual inductance arises. Due to the rotor position error, the measured position is not zero. In the transient state, the estimated position deviates from the reference value. The position controller sets a high q-current until the deviation from the reference value is compensated. In this state, the highest rotor position errors of about 28° occur due to the high mutual inductance. Overall, the rotor position estimate remains stable. In Fig. 10, the result for the compensation of the mutual inductance via $\tilde{\gamma}_{\mathrm{MI}}$ is shown. The curves are plotted in the same way as the previous ones.

The compensation of the mutual inductance leads to a reduced rotor position error. In the steady states, it remains

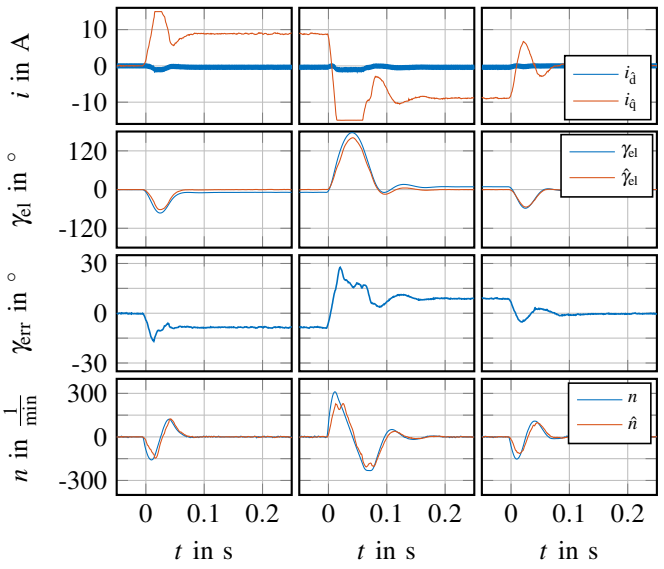

Figure 9: Closed-loop SSC in position control without compensation of the mutual inductance. Rated torque is applied (left), reversed (centre) and reduced to zero (right)

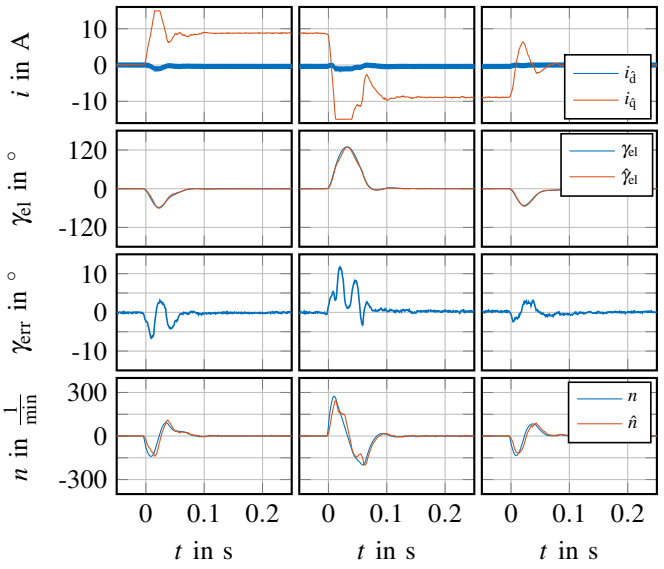

Figure 10: Closed-loop SSC in position control with compensation of the mutual inductance via $\tilde{\gamma}_{MI}$. Rated torque is applied (left), reversed (centre) and reduced to zero (right)

at 0°. Thus, the measured and estimated positions are set to the reference value of 0°. The maximum rotor position error is reduced to about 12°. An oscillatory rotor position error occurs in the transient states due to the multiple saliencies of the PMSM. Fig. 11 shows the result with compensation of the mutual inductance via L'_{dq} in the residual of the estimator.

The results of the two compensation methods are similar. There are only minor differences in the error of the rotor position estimate. Due to the fact that both methods achieve

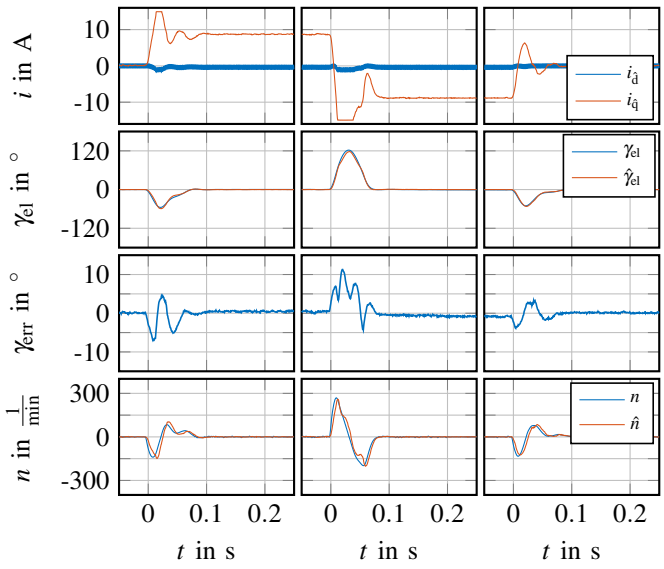

Figure 11: Closed-loop SSC in position control with compensation of the mutual inductance via L'_{dq} in ${}^{(\hat{d}\hat{q})}\vec{r}_{FDE}$. Rated torque is applied (left), reversed (centre) and reduced to zero (right)

similar results, the compensation using L'_{dq} in the residual is considered to be advantageous, as it is possible to ride through the point with identical self-inductances provided that sufficient mutual inductance is present. This advantage will be validated in future work.

VI. Conclusion

The comparison of the compensation methods for the error caused by the mutual inductance in the estimation of the rotor position shows that the mutual inductance can be compensated either via pre-rotation or via the consideration of the mutual inductance in the residual. Moreover, the mutual inductance can be used as a source of information in an SSC method based on numerical optimisation. Simulations show that the SSC is possible even with identical self-inductances of the d-axis and q-axis as long as a sufficiently large mutual inductance is present. In the experimental results, by considering the mutual inductance in the residual, the stationary rotor position estimation error is reduced, thus proving the functionality. In future work, the ride through of this point will be validated experimentally.

Acknowledgement

This work was funded by the Deutsche Forschungsgemeinschaft (DFG, German Research Foundation) – project identification number 424944120.

References

[1] S. Kim, J.-I. Ha, and S.-K. Sul, "PWM Switching Frequency Signal Injection Sensorless Method in IPMSM," *IEEE Transactions on Industry Applications*, vol. 48, no. 5, Sep. 2012.

[2] P. Landsmann, D. Paulus, A. Dötlinger, and R. Kennel, "Silent injection for saliency based sensorless control by means of current oversampling," in *2013 IEEE International Conference on Industrial Technology*, Feb. 2013.

[3] M. Berto, L. Alberti, and S. Bolognani, "Experimental Investigation on the Self-Sensing Capability of Synchronous Machines for Signal Injection Sensorless Drives," in *2021 IEEE Energy Conversion Congress and Exposition (ECCE)*, Oct. 2021.

[4] P. Guglielmi, M. Pastorelli, and A. Vagati, "Cross-Saturation Effects in IPM Motors and Related Impact on Sensorless Control," *IEEE Transactions on Industry Applications*, vol. 42, no. 6, Nov. 2006.

[5] N. Bianchi, E. Fornasiero, and S. Bolognani, "Effect of Stator and Rotor Saturation on Sensorless Rotor Position Detection," *IEEE Transactions on Industry Applications*, vol. 49, no. 3, May 2013.

[6] Y. Li, Z. Q. Zhu, D. Howe, C. M. Bingham, and D. A. Stone, "Improved Rotor-Position Estimation by Signal Injection in Brushless AC Motors, Accounting for Cross-Coupling Magnetic Saturation," *IEEE Transactions on Industry Applications*, vol. 45, no. 5, Sep. 2009.

[7] G. Lindemann, N. Himker, and A. Mertens, "Enhanced Observer with Adaptive Reference Frame for Self-Sensing Control of PMSM," in *2019 IEEE 10th International Symposium on Sensorless Control for Electrical Drives*, Sep. 2019.

[8] N. Himker, G. Lindemann, K. Wiedmann, B. Weber, and A. Mertens, "A Family of Adaptive Position Estimators for PMSM Using the Gradient Descent Method," *IEEE Journal of Emerging and Selected Topics in Power Electronics*, vol. 10, no. 2, Apr. 2022.

[9] P. Sergeant, F. De Belie, and J. Melkebeek, "Rotor Geometry Design of Interior PMSMs With and Without Flux Barriers for More Accurate Sensorless Control," *IEEE Transactions on Industrial Electronics*, vol. 59, no. 6, Jun. 2012.

[10] N. Himker and A. Mertens, "Analytical Design of Self-Sensing Control for PMSM Using Quasi-Direct Calculation," *IEEE Open Journal of Industry Applications*, vol. 4, 2023.

[11] D. Diaz Reigosa, P. Garcia, D. Raca, F. Briz, and R. D. Lorenz, "Measurement and Adaptive Decoupling of Cross-Saturation Effects and Secondary Saliencies in Sensorless Controlled IPM Synchronous Machines," *IEEE Transactions on Industry Applications*, vol. 44, no. 6, Nov. 2008.